Original Article

Assessment of Dose Calculation Accuracy of TiGRT Treatment Planning System Versus BEAMnrc Simulation in Nasopharyngeal Carcinoma: A Phantom study

Abstract

Background: Accurate dose calculations in radiotherapy are essential, especially in complex anatomical areas such as the nasopharynx, where heterogeneous tissue compositions can greatly influence treatment outcomes. This study assesses the accuracy of the full scatter convolution (FSC) algorithm within the TiGRT treatment planning system by comparing it to the BEAMnrc Monte Carlo (MC) simulation using a head phantom. **Methods:** EBT3 film was strategically placed in the nasopharyngeal region to enable direct comparisons between experimental results and those derived from the FSC and MC methods. Various metrics, including the dose difference index, two-dimensional gamma index, and horizontal and vertical dose profiles, were employed for the analysis. The heterogeneous regions were classified into bone, air, and soft-tissue components. For dosimetric evaluation, the irradiated areas were segmented into four regions based on isodose values: Field region (FR), irradiated region (IR), penumbra region (PR), and out-of-FR (OOFR). **Results:** The greatest computational discrepancies observed between the FSC algorithm and MC simulations in the air region of the FR were −5.12% ± 1.10% and 1.93% ± 1.45%, respectively. Notable underestimations occurred in the air and soft-tissue regions of the IR, PR, and OOFR when using the FSC algorithm, with a minimum discrepancy of −9.33% ± 5.51% and a maximum of −77.28% ± 8.19%. Conversely, doses calculated for the bone region were overestimated by 53.64% ± 5.65%. In comparison, the MC calculations in the IR region revealed discrepancies of 1.90% ± 1.55% (air), including a maximum underestimation of −8.82% ± 1.18% in the bone area within the PR. The gamma pass rates for different tissue types under local and global modes, using 3%-3 mm gamma criteria, demonstrate that the MC method consistently outperformed the TiGRT method across all tissue types, especially in the air (99.9%) and bone (99.8%) regions. **Conclusions:** The findings reveal that the FSC algorithm tends to underestimate doses in soft tissue and air while overestimating doses in bone. In contrast, there was excellent agreement between MC calculations and experimental measurements, highlighting the FSC algorithm's lower consistency.

Keywords: *BEAMnrc, EBT3 film, gamma index, nasopharyngeal carcinoma, TiGRT treatment planning system*

Submitted: 20-Dec-2024 **Revised:** 26-Apr-2025 **Accepted:** 09-Jun-2025 **Published:** 01-Nov-2025

Seyed Salman Zakariaee[1], Fereshteh Koosha[2], Mostafa Robatjazi[3], Hamed Rezaeejam[4], Mikaeil Molazadeh[5,6]

[1]Department of Medical Physics, Faculty of Paramedical Sciences, Ilam University of Medical Sciences, Ilam, Iran, [2]Department of Radiology Technology, Faculty of Allied Medical Sciences, Shahid Beheshti University of Medical Sciences, Tehran, Iran, [3]Department of Medical Physics and Radiological Sciences, Sabzevar University of Medical Sciences, Sabzevar, Iran, [4]Department of Radiology Technology, School of Paramedical Sciences, Zanjan University of Medical Sciences, Zanjan, Iran, [5]Medical Radiation Sciences Research Center, Tabriz University of Medical Sciences, Tabriz, Iran, [6]Department of Medical Physics, Faculty of Medicine, Tabriz University of Medical Sciences, Tabriz, Iran

Address for correspondence:
Dr. Mikaeil Molazadeh, Department of Medical Physics, Faculty of Medicine, Tabriz University of Medical Sciences, Tabriz, Iran.
E-mail: mikaeel.mollazadeh@gmail.com

Access this article online

Website: www.jmssjournal.net

DOI: 10.4103/jmss.jmss_87_24

Quick Response Code:

Introduction

In radiotherapy, dose calculation algorithms are employed to estimate the radiation dose delivered to target tissues and organs at risks. The rapid advancements in computational technology have led to the development of various algorithms designed to accurately model dose distributions. To ensure that these algorithms yield reliable results, it is essential to evaluate their performance across diverse media (such as air, soft tissue, lungs, and bones) and different modalities of ionizing radiation (including photons, protons, and electrons). An effective algorithm should comprehensively account for both primary and secondary dose contributions, particularly in the transport of secondary electrons through heterogeneous environments. Understanding the inherent uncertainties of these algorithms and validating their accuracy in dose computations is critical for establishing their clinical credibility.

The head-and-neck region, particularly the nasopharynx, presents the unique challenges for accurate dose calculation

How to cite this article: Zakariaee SS, Koosha F, Robatjazi M, Rezaeejam H, Molazadeh M. Assessment of dose calculation accuracy of TiGRT treatment planning system versus BEAMnrc simulation in nasopharyngeal carcinoma: A phantom study. J Med Sign Sens 2025;15:30.

due to its complex anatomy and heterogeneous tissue composition.[1-5] A significant limitation of many algorithms is their inability to adequately model changes in electron transport, leading to discrepancies of 10% or more in low/high-density regions such as air cavities and bones.[6,7] Such variations can result in clinically significant differences in treatment plans when comparing different algorithms.

Previous studies have examined the accuracy of dose distribution calculations using the pencil beam algorithm in the TiGRT treatment planning system (TPS) across various radiation fields (in-field, penumbra, and out-of-field) with different dosimetric tools, such as thermoluminescent dosimeter (TLD), ion chamber, and film.[8,9] However, these analyses have primarily focused on one-dimensional evaluations or limited point-by-point comparisons, with comprehensive two-dimensional (2D) or three-dimensional assessments being relatively rare.[4,10,11]

One of our objectives is to discern the strengths and weaknesses of the full scatter convolution (FSC) algorithm in comparison to Gafchromic film (GF) measurements and Monte Carlo (MC) calculations. The novelty of our study lies in the segmentation of various regions (air, soft tissue, and bone) and the assessment of the accuracy of TiGRT and MC dose distribution computations against practical measurements. This is achieved by isolating the segmented regions and analyzing them according to the specified isodose areas.

The present study aimed to rigorously evaluate the 2D accuracy of the FSC dose calculation algorithm in the TiGRT TPS against BEAMnrc MC simulations within a heterogeneous nasopharyngeal region. By employing practical measurements from GF in an anthropomorphic head-and-neck phantom, we conducted a detailed analysis of irradiated areas, utilizing various indices (dose difference [DD] index, vertical and horizontal dose profiles, and gamma index) to assess dose distribution accuracy. All irradiated areas within a slice of the nasopharyngeal heterogeneous region, including the field area, penumbra region (PR), and areas outside the radiation field, were examined in the context of air, soft tissue, and bone heterogeneity. In addition, dosimetric parameters for each heterogeneous region were analyzed separately.

In summary, the primary objective of this study is to comprehensively evaluate the 2D accuracy of the FSC algorithm in the TiGRT TPS by comparing it to BEAMnrc MC simulations within a heterogeneous nasopharyngeal region.

Materials and Methods

TiGRT treatment planning

A heterogeneous head-and-neck phantom, designed to replicate human anatomical features, was utilized for the treatment planning. This phantom was incorporating soft tissue, air, and bone heterogeneities. Plexiglass plates with a mass density of 1.18 g/cm^3 were employed to simulate soft tissue, while Polytetrafluoroethylene plates with a density of 2.18 g/cm^3 were representing bone.

The treatment plan was performed using the forward planning technique with TiGRT software (Targeted Image-guided Radiotherapy, LinaTech Co., Sunnyvale, CA, USA), version 1.0.10.573. Treatment protocols for nasopharyngeal carcinoma recommend a definitive radiotherapy dose of 70 Gy for high-risk clinical target volumes (CTV) and 50–60 Gy for low-to intermediate-risk CTVs, typically delivered in daily fractions of 2 Gy.[12-14] Given that high doses exceed the effective range of GFs, we applied a reduced dose of 600 cGy for our study, as lower doses have a higher error rate.[15] The isocenter was positioned within the soft tissue of the phantom, with the prescribed dose of 600 cGy administered at this point using a 6 MV linear accelerator (Oncor, Siemens AG, Erlangen, Germany). Two radiation fields, each measuring 15 cm × 15 cm, were applied at gantry angles of 90° and 270°, with equal beam weights. The dose calculations were performed using the FSC algorithm, and a voxel size of 1 mm^3 was selected for the dose matrix. The calculated monitor units for the right and left lateral fields were 349 and 343, respectively. An axial image of the phantom, illustrating the radiation fields at the isocenter slice, is presented in Figure 1b.

Monte Carlo simulation

The BEAMnrc code was utilized to simulate the radiotherapy machine, which was subsequently employed for dose distribution calculations following validation and verification procedures. The validation of our study simulations followed the methodology described by Sheikh-Bagheri *et al*.,[16] which involved comparing percentage depth dose and lateral dose profile curves across various field sizes. Our simulation results demonstrated a strong agreement between the curves derived from MC calculations and the experimental measurements.[5] The parameters for the incident electron energy and beam width were determined to be E = 6.2 MeV and full width at half maximum = 0.09 mm, respectively.[5] Each radiation field received irradiation from 1×10^9 electron particles directed at the accelerator target. A phase space file was generated at a distance of 70 cm from the target, resulting in a file size of 140 GB, containing 4.9×10^9 particles.

For dose computations in the MC simulations, DICOM computed tomography **(**CT) images (with a resolution of 1 mm^3) were processed using the DOSXYZnrc code via the CTCREATE program. Each radiation field irradiated the phantom's surface with 35×10^9 particles, totaling 70×10^9 particles for the entire phantom head. The uncertainty in the MC calculations was <0.5% (1 SD) based on the number of particles used in the simulation.

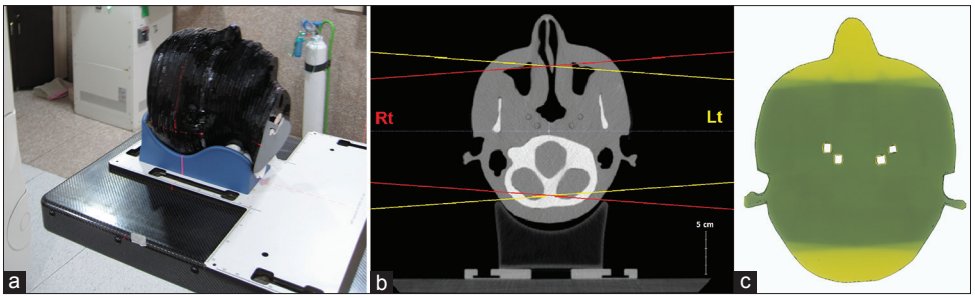

Figure 1: View of the head phantom on the treatment table (a). Computed tomography image of anthropomorphic head phantom with two opposite lateral fields (b) and scanned image of the irradiated Gafchromic film (c)

Variance reduction techniques were employed in the MC simulations to enhance computational efficiency and reduce processing time. The total cutoff energies for photon and electron particles were set at 0.01 MeV and 0.7 MeV, respectively, with energy saving parameters configured to 2 MeV. In addition, directional bremsstrahlung splitting was implemented to increase the photon yield from the linear accelerator target, with the number of bremsstrahlung splitting set to 1000.[17,18]

Practical measurements with EBT3 film

To obtain experimental planar dose distributions, an EBT3 film sheet was positioned axially at the isocenter within the phantom. The outer edges of the one sheet of GF were trimmed to conform to the shape and external dimensions of the phantom for the specified slice. To prevent any movement or rotation of the GF within the phantom, four holes were drilled at the center of the GF, allowing it to be secured in place using cylindrical rods embedded in the head phantom. The phantom was then irradiated according to the planned two lateral radiation fields [Figure 1a]. After irradiation, the GF was removed and stored in darkness. Following a 48–h period to allow for polymerization of the sensitive layer, the GF was scanned. Figure 1c displays the scanned GF after irradiation.

To convert the optical density (OD) of the irradiated GFs into absorbed dose, a calibration curve derived from GFs was utilized. Calibration GFs were cut into 5 cm × 5 cm pieces and irradiated under the reference conditions (radiation field size of 10 cm × 10 cm, distance of 100 cm from the phantom surface, and a depth of 5 cm in solid water). The GFs were exposed at the intervals of 0.5 Gy, ranging from 0 to 10 Gy. The *net*OD values were measured using a Microtek 9800XL scanner with a spatial resolution of 127 dpi (0.2 mm). The *net*OD values were then converted to absorbed doses using the calibration curve in the red channel. To ensure the reproducibility of each dose level on the calibration curve and the dose distributions obtained from phantom irradiation, measurements were repeated three times. The propagation of these uncertainties resulted in a *net*OD uncertainty of $< \pm 1\%$.

After acquiring the 2D dose distributions from the GF and MC simulations, horizontal and vertical dose profiles traversing heterogeneous tissue environments (soft tissue, air, and bone) were selected for comparison with the TiGRT dose profiles. We employed the gamma index to evaluate the concordance between the measured and calculated dose distributions. This index offers a quantitative measure of how closely the delivered dose aligns with the planned dose, factoring in both spatial and dosimetric variations with parameters called distance-to-agreement (DTA) and DD,[19] respectively. The gamma index is classified into two categories: local and global. The local gamma index assesses the agreement at each specific point within the dose distribution, comparing the dose at a given location in the measured distribution with the corresponding dose in the calculated distribution. In contrast, the global gamma index evaluates the overall agreement between the two dose distributions across the entire volume of interest, taking into account the complete dataset rather than focusing on individual points. A 2D gamma index was employed to analyze the data, evaluating all planar dose distributions relative to the reference dose distribution (EBT3 Film) using the standard acceptance criteria of 3%-3 mm in both global and local modes. The PTW VeriSoft software (MEPHYSTO software version 5.1, PTW, Freiburg, Germany) was utilized to calculate the gamma index, and the %DD index was also employed to assess dose discrepancies.

Results

%Dose difference index

For both quantitative and qualitative data analysis using the %DD index, the irradiated areas within the different regions (air, soft tissue, and bone) were categorized into four sections based on isodose levels:

- Field region (FR): Isodose areas exceeding 80%
- Irradiated region (IR): Isodose areas exceeding 20%
- PR: Isodose areas between 80% and 20%
- Out-of-FR (OOFR): Isodose areas below 20%.

Table 1 provides the details on each heterogeneous area and the percentage representation of each section within the four defined regions. The number of evaluated points in the FR, IR, PR, and OOFR was 23,084, 25,054, 1970, and 5499, respectively. In total, 30,553 points were assessed, with

contributions from air, soft tissue, and bone areas amounting to 4863, 20923, and 4767 points, respectively. A 2D map illustrating the %DD, which quantitatively and qualitatively expresses the percentage difference between the calculated doses from the MC code and the FSC algorithm compared to the measured dose distribution, is shown in Figure 2. For a more detailed analysis of the data in each heterogeneous region and to investigate DDs across the four defined irradiated areas, %DD index values were calculated between MC and GF calculations, as well as between TiGRT and GF calculations, using MATLAB software (R2015a). The equation used for calculating %DD is as follows:

$$\%DD = \frac{D_{cal} - D_{Ref}}{D_{Ref}} \times 100 \quad (1)$$

In this equation, D_{cal} represents the calculated dose (MC or TiGRT) and D_{ref} denotes the reference dose.

Figure 3 illustrates the %DD index values for both the MC method and the TiGRT algorithm in heterogeneous tissues. The analysis of the four defined regions presented in Figure 3 indicates that the TiGRT dose calculation algorithm significantly underestimates doses in heterogeneous regions characterized by air and soft tissue, particularly in the IR, PR, and the OOFR. In contrast, the FSC algorithm tends to overestimate doses in the bone region across these areas, leading to considerable discrepancies in the OOFR. Despite the claims made in the TiGRT user manual, which asserts that the system comprehensively accounts for the transport of all primary and secondary particles, including scattered particles such as secondary electrons, our findings suggest that the FSC algorithm falls short in accurately modeling beam behavior and exhibits the limitations in calculating dose distributions within heterogeneous environments, particularly concerning electronic equilibrium considerations. In addition, histogram graphs were generated for each area individually to illustrate the distribution of dose density [Figure 4].

Table 1: Surface area of different tissues (cm^2) and their percentages in different irradiated areas

	Air (%)	Soft tissue (%)	Bone (%)	Sum (cm^2)
Total area	48.6 (15.9)	209.2 (68.5)	47.7 (15.6)	305.5
FR	35.4 (15.3)	158.4 (68.6)	37.1 (16.1)	230.9
PR	2.7 (13.7)	14.5 (73.6)	2.5 (12.7)	19.7
IR	38.1 (15.2)	172.9 (69)	39.6 (15.8)	250.6
OOFR	10.5 (19.1)	36.3 (66.1)	8.1 (14.8)	54.9

FR – Field region; PR – Penumbra region; IR – Irradiated region; OOFR – Out-of-field region

Gamma index

The gamma index serves as another parameter for evaluating dose distribution maps, incorporating the DTA criteria alongside the %DD index. In this study, the gamma index was utilized not only to assess the overall dose distribution but also to evaluate the agreement of dose distributions within each heterogeneous region separately. The air, soft tissue, and bone regions were analyzed independently [Figure 5], and the dose distributions from both MC and TiGRT were compared to the reference dose distribution using a 3%-3 mm acceptance criterion in global and local modes. Figure 5 illustrates the gamma pass rate (GPR) in local mode for various inhomogeneous areas (both separately and collectively). The results of the data analysis are summarized in Table 2.

Vertical and horizontal dose profiles

From the dose distributions obtained through GF, MC, and TiGRT, four dose profiles along the horizontal and vertical directions, all incorporating heterogeneities, were selected for examination. The graphs of these profiles are presented in Figure 6. A summary of the results from the comparison of dose profiles is provided in Table 3. The data in Table 3 indicate a strong agreement between the MC calculations

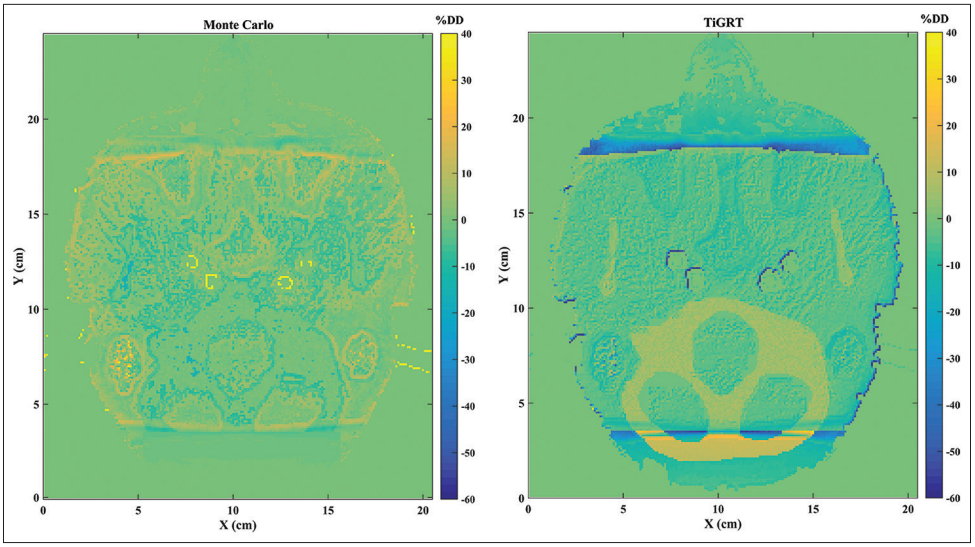

Figure 2: %Dose difference map for Monte Carlo and TiGRT

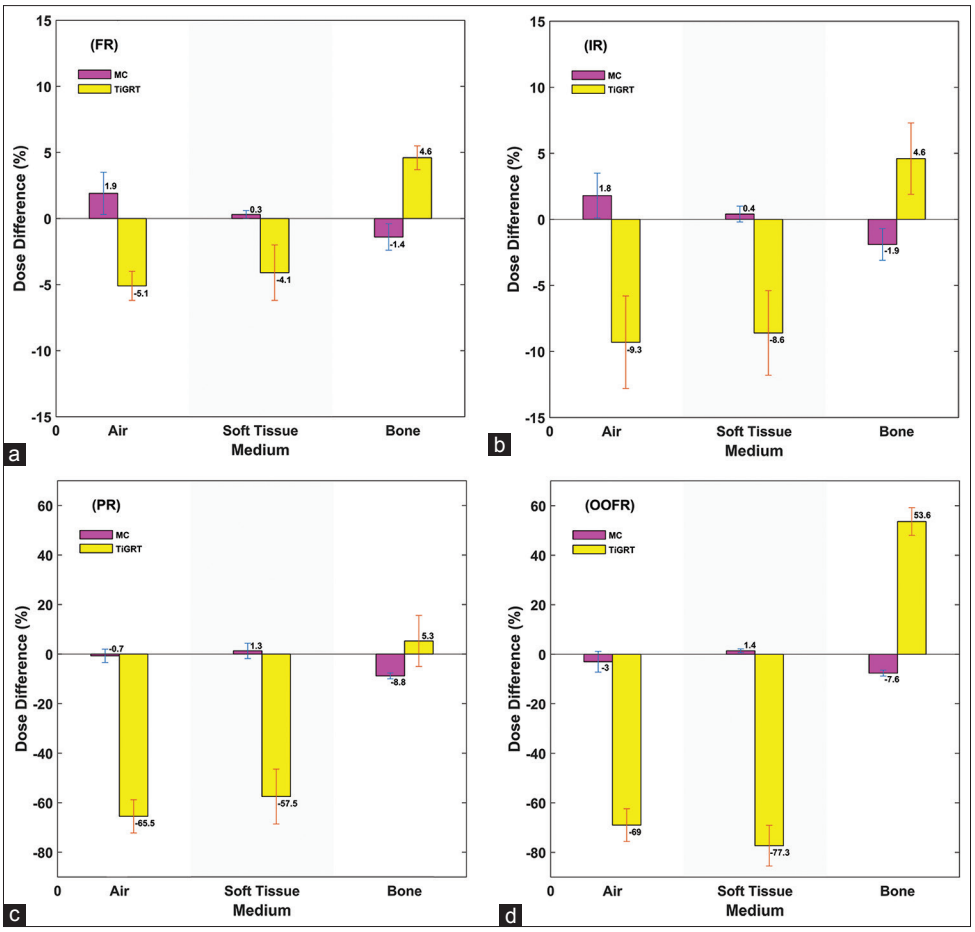

Figure 3: % Dose difference index values of Monte Carlo (MC) and TiGRT in the heterogeneous tissues. The color bars represent the relative differences in the mean absorbed dose (± SD) between MC and TiGRT relative to the Gafchromic film measurements for air, soft tissue, and bone regions in field region (a), irradiated region (b), penumbra region (c), and out-of-field region (d)

Table 2: Gamma pass rate of different parts of tissues in local and global modes

	Air	Soft tissue	Bone	Total
Local				
MC	99.9	94.4	99.3	98.6
TiGRT	66.2	85.2	79.8	78.6
Global				
MC	99.9	95.7	99.8	99.2
TiGRT	81.6	99.0	92.3	91.7

MC – Monte carlo; TiGRT – Targeted image guided radiotherapy

and the empirical measurements in the evaluation of the dose profiles.

Overall, our results indicate that the MC method significantly outperforms the TiGRT's FSC algorithm in accuracy, particularly in heterogeneous environments, highlighting the need for improved modeling of complex tissue interactions and particle transport in TiGRT TPS.

Discussion

In this study, to evaluate the accuracy of dose computational systems (TiGRT and MC), we employed a GF with a sufficient number of measurement points (with a spatial resolution of 1 mm) to obtain reliable results. However, the use of vertical and horizontal dose profiles alone may not adequately reflect the computational accuracy of dose calculation algorithms or determine their over/underestimation in heterogeneous tissues, so we evaluated the 2D dose distribution. In fact, with the help of the gamma index tool, we were able to analyze dose fluctuations in each heterogeneous area independently.

As illustrated in Figure 3a and b, the differences between the MC calculations and measurements in the FR and IR across all three disparate regions were consistently about 1.93% ± 1.45%. The smallest discrepancies were observed in soft tissue, while the greatest deviations were noted in the air (overestimation) and bone (underestimation) regions. In contrast, the differences between the TiGRT calculations and measurements in the FR and IR for these regions ranged from −9.33% ± 5.51% to 4.61% ± 2.69%, with the minimum difference again found in soft tissue, and most discrepancies occurring in the air region.

According to Figure 3c, the differences in MC calculations within the PR for air and soft tissue were

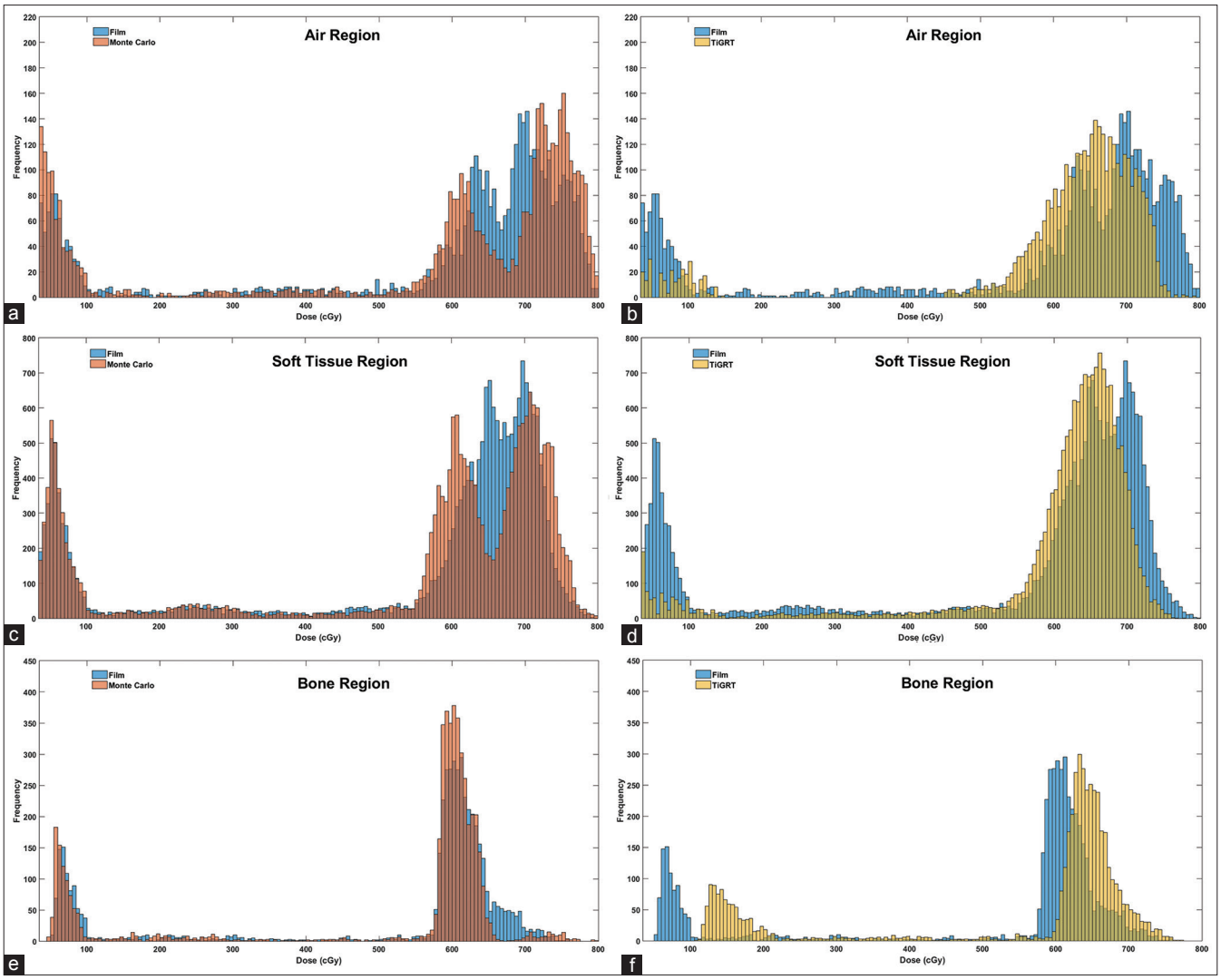

Figure 4: Histogram diagrams for the air (a and b), soft tissue (c and d), and bone (e and f) regions were derived from Gafchromic film measurements, Monte Carlo simulations, and full scatter convolution calculations

Table 3: The results of analysis of the horizontal and vertical dose profile diagrams related to Monte Carlo and targeted image guided radiotherapy (full scatter convolution) compared to gafchromic film by separating inhomogeneous regions

	Air	Soft tissue	Bone
MC (profile A)	2.15±3.67	−2.81±2.27	−1.37±1.84
FSC (profile B)	−3.71±4.15	2.10±3.14	2.55±3.45
MC (profile C)	0.14±1.94	0.29±1.72	−1.68±2.08
FSC (profile D)	−13.24±5.55	−3.56±3.47	−3.38±3.63

Values are reported as the average percentage difference±SD.
FSC – Full scatter convolution; MC: Monte Carlo; SD – Standard deviation

<1.38% ± 2.75%, but the discrepancy for the bone reached to −8.82% ± 1.24%. Conversely, the FSC algorithm exhibited substantial differences in the same region, with air showing a maximum underestimation of −65.51% ± 6.74% and soft tissue at −57.57% ± 1.16%.

Data presented in Figure 3d indicate that the computational differences in the OOFR for the MC method were significantly smaller than those from the TiGRT's point kernel algorithm. In the MC calculations, the largest discrepancies were observed in the bone regions, with differences reaching −7.63% ± 0.20%. For the FSC algorithm, the maximum and minimum discrepancies were noted in soft tissue (up to −77.33% ± 8.25%) and bone (up to 53.68% ± 5.66%), respectively. Previous studies by Huang *et al.* and Howell *et al.* have reported similar significant underestimations in other TPSs, such as Pinnacle and Eclipse, with discrepancies reaching 40%–50% in areas outside the radiation field.[20,21] This trend can also be seen in the histogram charts [Figure 4].

From the data in Table 2 and Figure 5, it is evident that the GPR index showed excellent agreement between MC and GF measurements in both local and global modes. However, the agreement between the FSC algorithm calculations and experimental measurements was acceptable in the global

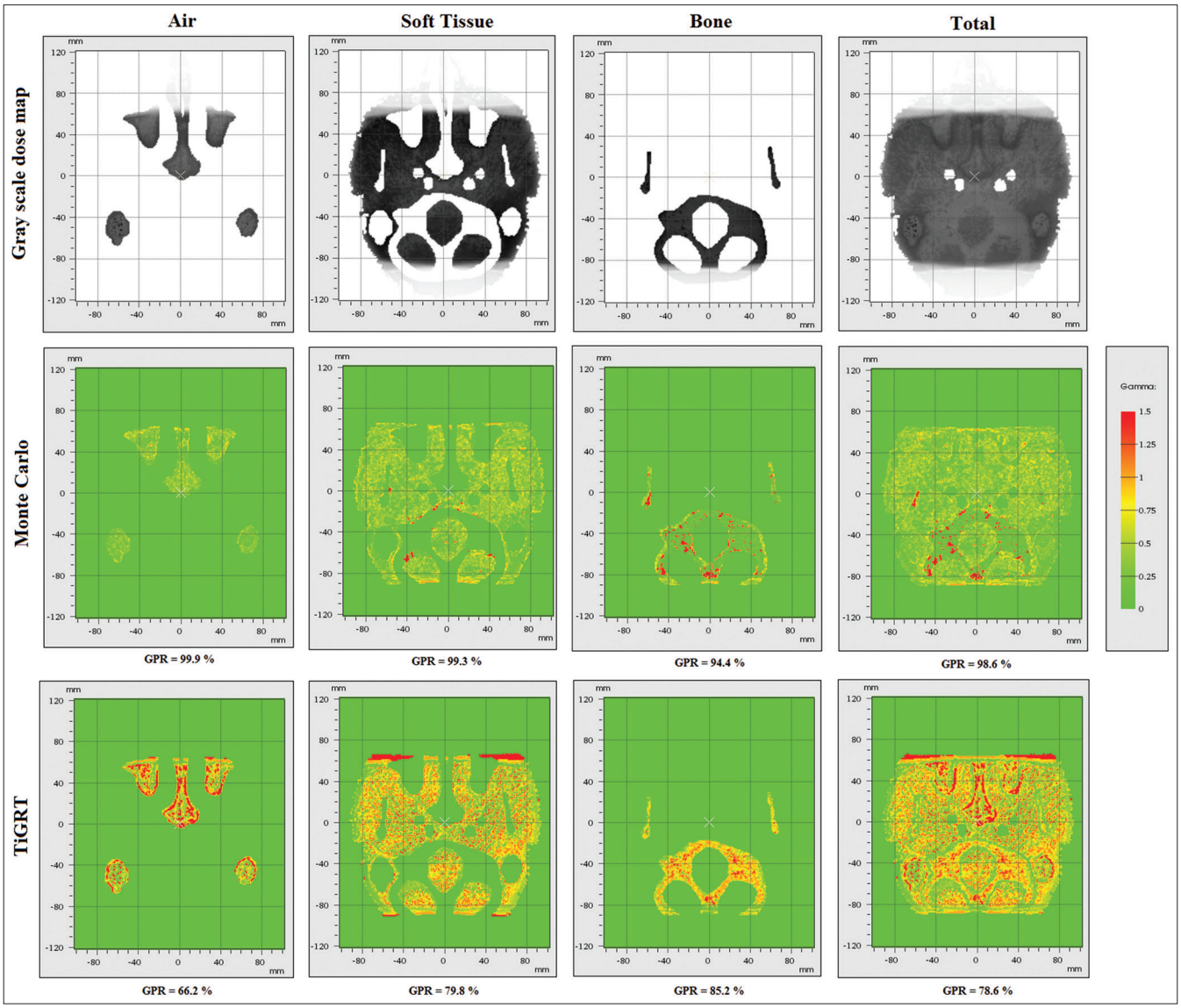

Figure 5: Images of different assorted zones (air, soft tissue, and bone) were segmented as gray scale dose maps (top row), and their related gamma pass rate s for the two-dimensional dose distribution map of Monte Carlo and TiGRT were compared with the experimental dose distribution of the Gafchromic film with 3%-3 mm gamma criteria in local mode (second and third rows)

mode but considerably weaker and unacceptable in the local mode. The results in Figure 5 indicate that the lowest GPR in the MC dose distribution occurred in the bone region (94.4%), while for TiGRT, the lowest and highest agreements were found in air (66.2%) and bone (85.2%), respectively.

Several factors contribute to the observed lower GPR in the TiGRT system compared to MC calculations in the heterogeneous areas, particularly in air. FSC algorithm face challenges in accurately modeling complex tissue heterogeneities, which can result in inaccuracies in dose distribution, especially in regions with varying densities (modeling limitations). In addition, dose calculations often rely on the assumption of electronic equilibrium, a condition that may not be met in heterogeneous environments, particularly at the interfaces between different tissue types (electronic equilibrium).

Furthermore, insufficient modeling of the transport of secondary particles, such as scattered electrons and photons, can lead to significant underestimations or overestimations of dose in specific regions (secondary particle transport). Inconsistent calibration of treatment machine, along with a lack of comprehensive validation against clinical outcomes, can introduce the errors in dose delivery (calibration and validation).

The presence of air pockets or cavities within or adjacent to treatment sites can also create substantial discrepancies in dose calculations, as the low density of air compared to surrounding tissues affects the accuracy of predictions (air-tissue interfaces). Finally, the limited accuracy of measurement techniques for air dose can impede the validation of dose calculation algorithms, given the challenges associated with obtaining direct measurements in air (measurement techniques).

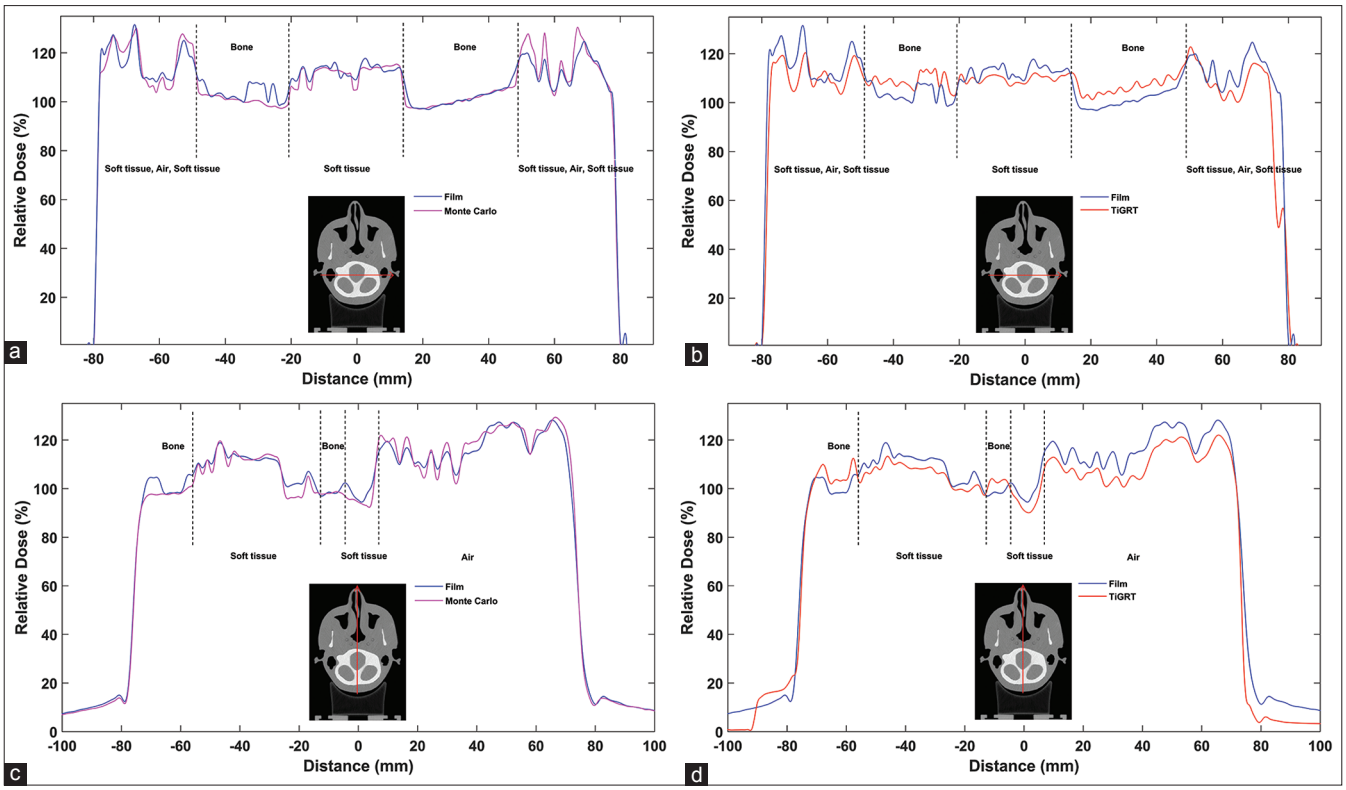

Figure 6: Diagrams comparing horizontal and vertical dose profiles between Gafchromic film measurements and Monte Carlo calculations (a and c), as well as between film measurements and the full scatter convolution algorithm (b and d)

The analysis of the four defined regions in Figure 3 reveals a significant underestimation in the TiGRT dose calculation algorithm in heterogeneous air and soft-tissue regions, particularly within the IR, PR, and OOFR. Conversely, the FSC algorithm tended to overestimate doses in the bone region across these areas, resulting in substantial differences in the OOFR. According to the TiGRT user manual, the system claims to fully account for the transport of all primary and secondary particles, particularly scattered particles (including secondary electrons). However, our findings suggest that the FSC algorithm lacks the capability to model beams accurately and has limitations in calculating dose distributions in heterogeneous environments with respect to electronic equilibrium considerations.

In a study by Abdemanafi *et al*.,[22] the accuracy of point dose determinations from the TiGRT TPS was evaluated using TLDs at ten distinct points within a heterogeneous thorax phantom (breast and lung areas). Their results indicated that the TPS system provided high dose estimations of 4% inside the radiation field and 4.5% outside the field for lung tissue.[22] Similarly, Bahreyni Toossi *et al*.[8] assessed the accuracy of the FSC TiGRT algorithm in the breast region using multiple TLDs in a RANDO (Radiation Anthropomorphic Non-homogeneous Dosimetry Object) phantom, revealing that the TPS calculations were significantly limited outside the radiation field, with an average underestimation of approximately 39%. In contrast, the average differences within the radiation field were within ± 5%.[8] Furthermore, computational differences inside and outside the radiation field in the lung tissue were 3.8% and −15%, respectively. These studies indicate inconsistencies in the accuracy of dose estimations from the TiGRT TPS outside the radiation field in lung heterogeneity, with varying results in terms of over/underestimation.

Bahreyni Toossi *et al*.[9] reported on the accuracy of FSC radiation dose assessments for the head and neck in a RANDO phantom, utilizing 47 TLD-100 chips. Their findings indicated acceptable computational differences (± 5%) in the heterogeneous tissues within the radiation field, but estimated discrepancies of −40% in the penumbra and out-of-field areas. Specifically, the differences within the radiation area were 2.6% for the soft tissue and 4% for bone, while outside the radiation field, discrepancies were −20% for the soft tissue and −17% for the bone. A significant difference of −31% was noted at four points in the penumbra region within the bone.[9] Notably, these studies were limited by the small number of dose points evaluated, making it challenging to draw definitive conclusions about the accuracy of TPS systems inside or outside the radiation field across various heterogeneous areas.

In our study, comparing the TiGRT results with those from the MC simulations indicates that the accuracy of calculations from the MC simulation significantly surpasses that of the FSC algorithm. This is expected, as

MC simulations utilize advanced mathematical methods (albeit time-consuming) to model particle transport and interactions, particularly in heterogeneous environments. Furthermore, MC simulations leverage precise tissue elements from a code library to calculate doses across different tissues (soft tissue, fat, muscle, soft bone, dense bone, lung, and air), and all necessary mass density information is derived from CT data. In contrast, model-centric algorithms typically use water as a reference material, applying corrections for dosimetric calculations based on changes in relative electron density obtained from CT data. According to the International Commission on Radiation Units and Measurements (ICRU) report No. 37[23] and the study by Siebers *et al*.,[24] converting absorbed doses in bone (dose-to-tissue) to absorbed doses in water (dose-to-water) using stopping power ratios reveals DDs of 3.5% for soft bone and 10% for dense bone relative to their electron densities. Consequently, dose modeling for corrected heterogeneous materials (relative to a reference water phantom) lack sufficient accuracy. Algorithms that compute dose distributions based on dose-to-medium rather than dose-to-water demonstrate higher computational accuracy.[2,3] Thus, the significant computational differences between treatment planning algorithms and MC are evident.

The FSC algorithm employs a convolution equation that simplifies physical processes by convolving the primary X-ray energy fluence with a kernel. While it accounts for side scattering of transmitted photons in heterogeneous media, the MC simulates all actual interaction phenomena, providing more precise dose modeling despite being time-consuming. However, MC calculations achieve accuracy under two conditions: First, the medical accelerator head must be accurately simulated and finely tuned using practical measurements; second, enough particles must be used during dose distribution extraction to ensure acceptable statistical uncertainty.

The primary objective of radiotherapy is to achieve optimal dose distribution, maximizing exposure to the tumor while minimizing radiation to normal and vital tissues. Both underdosing and overdosing can significantly impact treatment efficacy, affecting both target and surrounding tissues. Our study highlights areas where computational algorithms may produce dose estimation errors, allowing for a better understanding of their strengths and weaknesses in clinical applications. Decreasing the radiation dose to the tumor can lead to inadequate tumor control, resulting in incomplete cell kill and the potential survival of cancer cells, which may complicate treatment and increase the risk of local recurrence. Conversely, increasing the dose can enhance tumor control by promoting cell kill, but this must be carefully managed to avoid overdosing, which can cause significant toxicity and complications in normal tissues.

In cases where the tumor is in close proximity to air, lowering the radiation dose to airy areas like the sinuses can result in insufficient tumor control, as cancer cells may not receive adequate exposure. On the other hand, increasing the dose in these regions can lead to serious complications, including mucositis and inflammation, which can impair respiratory function. Long-term effects may include fibrosis, necrosis, and even secondary malignancies, with excessive radiation posing risks to nearby critical structures in the brain.

If the tumor involves soft tissue, reducing the dose may initially leave surrounding soft tissues unaffected, but the risk of incomplete tumor eradication remains, potentially allowing cancer cells to invade nearby tissues. Overdosing in these areas can cause acute side effects such as severe skin reactions and mucositis, leading to complications such as infection and delayed healing. Long-term consequences may include fibrosis and necrosis, complicating recovery.

Underdosing in bone tissue (in tumors involving bone tissue) may not have immediate effects compared to overdosing; however, it leaves tumors untreated, allowing for further growth and potential metastasis. This can complicate future treatment options and worsen the overall prognosis, emphasizing the need for careful dose management in radiotherapy.

Therefore, balancing the radiation dose to maximize tumor control while minimizing damage to normal tissues is crucial for effective radiotherapy. Accurate treatment planning and delivery, guided by advanced imaging and dosimetry, are essential to achieve optimal outcomes in cancer treatment.

Our study has several limitations related to phantom construction and uncertainties in film dosimetry. A key limitation in constructing anthropomorphic head phantoms is the simplification of anatomical structures. Although these phantoms are designed to replicate human anatomy, they often fail to accurately represent the complex geometry and tissue composition of the head. Variations in bone density, soft-tissue distribution, and the presence of air cavities, such as sinuses, can significantly affect dose distribution. Simplified models may overlook these factors, resulting in discrepancies between the phantom and actual patient anatomy.[25,26]

Furthermore, anthropomorphic phantoms usually employ homogeneous materials to simulate tissues, which can lead to considerable dosimetric errors. Human tissues vary not only in density but also in atomic composition, influencing their interaction with radiation. For example, differences in water content across the soft tissues can impact dose absorption, making uniform materials inadequate for accurate dose predictions.[27] In addition, the 5-mm slice thickness of these phantoms may not effectively capture the structural changes in tissues or small, sensitive organs such as the optic chiasm.

In terms of film dosimetry, calibration is essential for accurate dose measurements. Variations in film response

due to exposure conditions, such as temperature and humidity,[28] can introduce significant uncertainties. Moreover, radiochromic films exhibit energy dependence,[29] complicating dose assessments in treatments using varied energy beams. Processing after irradiation can also introduce uncertainties, as factors like the time before analysis and scanning methods[30] can affect measurement accuracy, leading to inconsistencies that may impact treatment planning.

Conclusions

This study evaluated the accuracy of dose estimations from the TiGRT TPS (FSC algorithm) and MC simulations in the presence of various heterogeneities within the nasopharyngeal region of a heterogeneous head phantom, relative to practical measurements. The results indicated that the dose profiles obtained from MC calculations aligned well with experimental profiles compared to those from the FSC algorithm. Furthermore, a comprehensive analysis of the 2D dose distribution using the gamma index demonstrated excellent agreement between MC computations and the reference dose distribution. However, the TiGRT results were less satisfactory in local mode, while they were somewhat acceptable in global mode. Overall, our research indicates that the FSC algorithm within the TiGRT software is unable to achieve precise radiation calculations in heterogeneous head-and-neck environments when compared to MC simulations. As a result, the dose distribution calculated using this algorithm in the nasopharyngeal region was found to be either overestimated or underestimated, depending on the region of interest.

Ethical approval

The Research Ethics Committees of Vice-Chancellor in Research Affairs-Tabriz University of Medical Sciences approved the study protocol (Ethic code: IR.TBZMED.VCR.REC.1403.163).

Funding

Financial support was provided by Vice-Chancellor in Research Affairs-Tabriz University of Medical Sciences [Grant number: 75168].

Availability of data and materials

The data of study are available on reasonable request.

Conflict of interest

The authors have no conflicts of interest.

Acknowledgments

The authors thank the staff of the Radiotherapy Department of Tabriz Madani Hospital especially Mr. Amin Pourfarshid for allowing access to the linear accelerator, TiGRT treatment planning system, and dosimetry equipment.

Authorship contribution statement

Seyed Salman Zakariaee: Term, Conceptualization, Methodology, Software, Validation, Formal analysis, Investigation, Data Curation, Writing - Original Draft. Fereshteh Koosha: Software, Phantom fabrication, Formal analysis, Investigation, Data Curation, Writing - Review & Editing. Mostafa Robatjazi: Term, Conceptualization, Software, Data Curation, Writing - Review & Editing. Hamed Rezaeejam: Software, Formal analysis, Writing - Original Draft. Mikaeil Molazadeh: Conceptualization, Methodology, Writing - Original Draft, Supervision, Project administration, Funding acquisition, Phantom fabrication.

References

1. Kan MW, Cheung JY, Leung LH, Lau BM, Yu PK. The accuracy of dose calculations by anisotropic analytical algorithms for stereotactic radiotherapy in nasopharyngeal carcinoma. Phys Med Biol 2011;56:397-413.
2. Radojčić ĐS, Kolacio MŠ, Radojčić M, Rajlić D, Casar B, Faj D, *et al.* Comparison of calculated dose distributions reported as dose-to-water and dose-to-medium for intensity-modulated radiotherapy of nasopharyngeal cancer patients. Med Dosim 2018;43:363-9.
3. Sayah R, Felefly T, Zouein L, El Barouky J, Khater N, Farah N, *et al.* Dosimetric impact of switching from AAA to acuros dose-to-water and dose-to-medium for RapidArc plans of nasopharyngeal carcinomas. Cancer Radiother 2020;24:842-50.
4. Molazadeh M, Robatjazi M, Geraily G, Rezaeejam H, Zeinali A, Shirazi A. Three-dimensional IMRT QA of Monte Carlo and full scatter convolution algorithms based on 3D film dosimetry. Radiat Phys Chem 2021;186:109528.
5. Molazadeh M, Zeinali A, Robatjazi M, Shirazi A, Geraily G. Dosimetric characteristics of LinaTech DMLC H multi leaf collimator: Monte Carlo simulation and experimental study. J Appl Clin Med Phys 2017;18:113-24.
6. Mesbahi A, Fix M, Allahverdi M, Grein E, Garaati H. Monte Carlo calculation of Varian 2300C/D Linac photon beam characteristics: A comparison between MCNP4C, GEANT3 and measurements. Appl Radiat Isot 2005;62:469-77.
7. Amankwaa-Frempong E, Vernimmen F, Blay S, Ezhilalan R. Irradiation of lung and esophagus tumors: A comparison of dose distributions calculated by anisotropic analytical algorithm and pencil beam convolution algorithm, a retrospective dosimetric study. Int J Cancer Ther Oncol 2014;2:1-6.
8. Bahreyni Toossi MT, Soleymanifard S, Farhood B, Mohebbi S, Davenport D. Assessment of accuracy of out-of-field dose calculations by TiGRT treatment planning system in radiotherapy. J Cancer Res Ther 2018;14:634-9.
9. Bahreyni Toossi MT, Farhood B, Soleymanifard S. Evaluation of dose calculations accuracy of a commercial treatment planning system for the head and neck region in radiotherapy. Rep Pract Oncol Radiother 2017;22:420-7.
10. Mahmoudi G, Farhood B, Shokrani P, Amouheidari A, Atarod M. Evaluation of the photon dose calculation accuracy in radiation therapy of malignant pleural mesothelioma. J Cancer Res Ther 2018;14:1029-35.
11. Zeinali A, Mahani L, Kargar N. Evaluation of full scatter convolution algorithm performance in the presence of inhomogeneities using a novel method of three-dimensional film dosimetry. Int J Radiat Res 2021;19:391-9.
12. Bossi P, Chan AT, Licitra L, Trama A, Orlandi E, Hui EP, *et al.*

Nasopharyngeal carcinoma: ESMO-EURACAN clinical practice guidelines for diagnosis, treatment and follow-up(†). Ann Oncol 2021;32:452-65.
13. Lee AW, Ng WT, Pan JJ, Poh SS, Ahn YC, AlHussain H, *et al.* International guideline for the delineation of the clinical target volumes (CTV) for nasopharyngeal carcinoma. Radiother Oncol 2018;126:25-36.
14. Ng WT, Chow JC, Beitler JJ, Corry J, Mendenhall W, Lee AW, *et al.* Current radiotherapy considerations for nasopharyngeal carcinoma. Cancers (Basel) 2022;14:5773.
15. Huang L, Gaballa H, Chang J. Evaluating dosimetric accuracy of the 6 MV calibration on EBT3 film in the use of Ir-192 high dose rate brachytherapy. J Appl Clin Med Phys 2022;23:e13571.
16. Sheikh-Bagheri D, Rogers DW. Sensitivity of megavoltage photon beam Monte Carlo simulations to electron beam and other parameters. Med Phys 2002;29:379-90.
17. Kawrakow I, Rogers DW, Walters BR. Large efficiency improvements in BEAMnrc using directional bremsstrahlung splitting. Med Phys 2004;31:2883-98.
18. Joosten A, Bochud F, Baechler S, Levi F, Mirimanoff RO, Moeckli R. Variability of a peripheral dose among various linac geometries for second cancer risk assessment. Phys Med Biol 2011;56:5131-51.
19. Low DA, Harms WB, Mutic S, Purdy JA. A technique for the quantitative evaluation of dose distributions. Med Phys 1998;25:656-61.
20. Huang JY, Followill DS, Wang XA, Kry SF. Accuracy and sources of error of out-of field dose calculations by a commercial treatment planning system for intensity-modulated radiation therapy treatments. J Appl Clin Med Phys 2013;14:4139.
21. Howell RM, Scarboro SB, Kry SF, Yaldo DZ. Accuracy of out-of-field dose calculations by a commercial treatment planning system. Phys Med Biol 2010;55:6999-7008.
22. Abdemanafi M, Tavakoli MB, Akhavan A, Abedi I. Evaluation of the lung dose in three-dimensional conformal radiation therapy of left-sided breast cancer: A phantom study. J Med Signals Sens 2020;10:48-52.
23. ICRU. Report No. 37, Stopping powers for electrons and positrons. Vol. 19. Bethesda, MD, USA: International Commission on Radiation Units and Measurements; 1984. p. 1-271.
24. Siebers JV, Keall PJ, Nahum AE, Mohan R. Converting absorbed dose to medium to absorbed dose to water for Monte Carlo based photon beam dose calculations. Phys Med Biol 2000;45:983-95.
25. Lai M, Skyrman S, Kor F, Homan R, El-Hajj VG, Babic D, *et al*. Development of a CT-compatible, Anthropomorphic skull and brain phantom for neurosurgical planning, training, and simulation. Bioengineering (Basel) 2022;9:537.
26. Holmes RB, Negus IS, Wiltshire SJ, Thorne GC, Young P, Alzheimer's Disease Neuroimaging Initiative. Creation of an anthropomorphic CT head phantom for verification of image segmentation. Med Phys 2020;47:2380-91.
27. Breslin T, Paino J, Wegner M, Engels E, Fiedler S, Forrester H, *et al*. A novel anthropomorphic phantom composed of tissue-equivalent materials for use in experimental radiotherapy: Design, dosimetry and biological pilot study. Biomimetics (Basel) 2023;8:230.
28. Ningnoi T, Ehlermann D. Effects of temperature and humidity during irradiation on the response of radiachromic film dosimeters. Radiat Phys Chem 1994;43:569-72.
29. Devic S. Radiochromic film dosimetry: Past, present, and future. Phys Med 2011;27:122-34.
30. Devic S, Seuntjens J, Sham E, Podgorsak EB, Schmidtlein CR, Kirov AS, *et al.* Precise radiochromic film dosimetry using a flat-bed document scanner. Med Phys 2005;32:2245-53.